

Scaling approach to nuclear structure in high-energy heavy-ion collisions

Jiangyong Jia^{1,2,*} and Chunjian Zhang^{1,†}

¹*Department of Chemistry, Stony Brook University, Stony Brook, NY 11794, USA*

²*Physics Department, Brookhaven National Laboratory, Upton, NY 11976, USA*

In high-energy heavy-ion collisions, the energy density profile of the produced quark-gluon plasma and its space-time dynamics are sensitive to the shape and radial profiles of the nuclei, described by the collective nuclear structure parameters including quadrupole deformation β_2 , octupole deformation β_3 , radius R_0 and surface diffuseness a . Using hydrodynamic model simulations, we find a general scaling relation between these parameters and a large class of experimental observables such as elliptic flow v_2 , triangular flow v_3 and particle multiplicity distribution $p(N_{\text{ch}})$. In particular, we show that the ratio of these observables between two isobar collision systems depends only on the differences of these parameters. Using this scaling relation, we show how the nuclear structure parameters of $^{96}_{44}\text{Ru}$ and $^{96}_{40}\text{Zr}$ conspire to produce the non-monotonic centrality dependence of ratios of v_2 , v_3 and $p(N_{\text{ch}})$ between $^{96}_{44}\text{Ru}+^{96}_{44}\text{Ru}$ and $^{96}_{40}\text{Zr}+^{96}_{40}\text{Zr}$ collisions, in agreement with measurements by the STAR Collaboration. This scaling approach towards heavy-ion observables demonstrates that isobar collisions is a precision tool to probe the shape and radial structures, including the neutron skin, of the atomic nuclei across energy scales.

PACS numbers: 25.75.Gz, 25.75.Ld, 25.75.-1

One main challenge in nuclear physics is to map out the shape and radial structure of the atomic nuclei and understand how they emerge from the interactions among the constituent nucleons [1, 2]. Varying the number of nucleons along isotopic/isotonic chain often induces rich and non-monotonic changes in the nuclear structure properties. In certain regions of nuclear chart, for example, even adding or subtracting a few nucleons can induce significant deformations and/or changes in the nuclear radius or neutron skin [3–6]. Experimental information of nuclear structure is primarily obtained by spectroscopic or scattering measurements at low energies. But studies show that nuclear structure can be probed in high-energy nuclear collisions [7–21], and experimental evidences have been observed [22–26].

To see why heavy-ion collisions can be used to probe the nuclear structure, we refer to the cartoon in Fig. 1. These high-energy collisions deposit a large amount of energy in the overlap region, forming a hot and dense quark-gluon plasma (QGP) [27]. The shape and size of the initially formed QGP are mainly controlled by the impact parameter but are also affected by the shape and radial profile of the nucleon distribution in the colliding nuclei, often described by a deformed Woods-Saxon (WS) density,

$$\rho(r, \theta, \phi) \propto \frac{1}{1 + e^{[r - R_0(1 + \beta_2 Y_2^0(\theta, \phi) + \beta_3 Y_3^0(\theta, \phi))/a]}}, \quad (1)$$

where the nuclear surface includes only the most relevant axial symmetric quadrupole deformation β_2 and octupole deformation β_3 . R_0 is the half-density nuclear radius, and a is the surface diffuseness which is sensitive to the neutron skin [28]. The nuclear deformation β_2 (β_3) enhances the ellipticity (triangularity) of the overlap region [10, 20, 29], characterized by the eccentricity ε_2 (ε_3): $\varepsilon_n = |\int r^n e^{in\phi} r dr d\phi| / \int r^n r dr d\phi|$ from

position (r, ϕ) of participating nucleons [30]. The ε_2 (ε_3) drives the anisotropic elliptic flow v_2 (triangular flow v_3) of the produced particles following an approximate linear response relation $v_n \propto \varepsilon_n$ in each collision event [31]. A change in a is found to not only influence the ε_n but also the charge particle multiplicity distribution $p(N_{\text{ch}})$ [12, 32]. The impact of a variation in R_0 on final-state observable has not yet been explicitly studied.

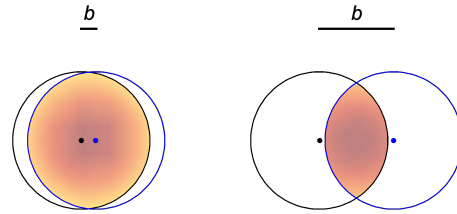


FIG. 1. Initial transverse geometry of heavy-ion collisions with small (left) and large (right) impact parameter b . The dots indicate the center of the nuclei and the filled area indicates the overlap region where the QGP is formed. Clearly, the initial geometry of the QGP depends on the shape and radial profile of colliding nuclei and the b .

Due to the dominant role of the impact parameter, earlier studies focused on the most central collisions where the shape of the overlap is more circular and the impact of nuclear deformation can be more easily identified. It is realized recently that the impact of nuclear structure can be cleanly isolated over the full centrality range by comparing two isobaric collision systems [17, 18]. Since isobar nuclei have the same mass number but different structure, deviation from unity of the ratio of any observable must originate from differences in the structure of the colliding nuclei, which impact the initial state of QGP and its final state observables. Collisions of one

such pair of isobar systems, $^{96}\text{Ru}+^{96}\text{Ru}$ and $^{96}\text{Zr}+^{96}\text{Zr}$, have been performed at RHIC. Ratios of many observables between the two isobar systems have been published by the STAR Collaboration, and they all show significant and centrality-dependent departures from unity [33]. The goal of this Letter is to explore the scaling behavior of these ratios with respect to the WS parameters in Eq. (1).

We illustrate the idea using three heavy-ion observables, the v_2 , v_3 and $p(N_{\text{ch}})$, although this idea applies to many other single-particle or two-particle observables. For small deformations and small variation of R_0 and a from their default reference values, the observable \mathcal{O} should have a simple leading-order dependence,

$$\mathcal{O} \approx b_0 + b_1\beta_2^2 + b_2\beta_3^2 + b_3(R_0 - R_{0,\text{ref}}) + b_4(a - a_{\text{ref}}), \quad (2)$$

where $b_0 \equiv \mathcal{O}(R_{0,\text{ref}}, a_{\text{ref}})$ is the value for spherical nuclei with the reference radius and diffuseness, and b_1 – b_4 are centrality-dependent response coefficients that are encoded in the final-state dynamics. Note that the leading-order contribution from deformation appears as β_n^2 instead of β_n because these observables do not depend on the sign of β_n [20, 34]¹. The b_n coefficients depend on the mass number but otherwise are the same between isobars. Therefore, the ratio of \mathcal{O} between $^{96}\text{Ru}+^{96}\text{Ru}$ and $^{96}\text{Zr}+^{96}\text{Zr}$ follows a simple scaling relation

$$R_{\mathcal{O}} \equiv \frac{\mathcal{O}_{\text{Ru}}}{\mathcal{O}_{\text{Zr}}} \approx 1 + c_1\Delta\beta_2^2 + c_2\Delta\beta_3^2 + c_3\Delta R_0 + c_4\Delta a. \quad (3)$$

where $\Delta\beta_n^2 = \beta_{n,\text{Ru}}^2 - \beta_{n,\text{Zr}}^2$, $\Delta R_0 = R_{0,\text{Ru}} - R_{0,\text{Zr}}$, and $\Delta a = a_{\text{Ru}} - a_{\text{Zr}}$. This ratio can thus probe the difference in the WS parameters between the isobar nuclei.

Our main finding is that the Eq. (3) works well over a wide range of parameters. The coefficients c_n can be obtained precisely by inputting a large parameter in a given model. The extracted c_n can then be used to predict $R_{\mathcal{O}}$ for any other values of $\Delta\beta_n^2$, ΔR_0 and Δa .

We simulate the dynamics of the QGP using the multi-phase transport model (AMPT) [35] as a proxy for hydrodynamics. The AMPT model has proven successful in describing collective flow data in small and large collision systems at RHIC and the LHC [36, 37] and has been used to study the β_n dependence of v_n [18, 38]. We use AMPT v2.26t5 in string-melting mode at $\sqrt{s_{\text{NN}}} = 200$ GeV with a partonic cross section of 3.0 mb [39, 40]. We simulate generic isobar $^{96}\text{X}+^{96}\text{X}$ collisions covering a wide ranges of β_2 , β_3 , R_0 and a , including the default values assumed for ^{96}Ru and ^{96}Zr listed in Table I. Following Ref. [41], the default values are taken from Ref. [42] for R_0 or deduced from neutron skin data [43] for a . The default values of β_2 and β_3 are taken from Ref. [38] but slightly

modified. The v_n are calculated using two-particle correlation method with hadrons of $0.2 < p_{\text{T}} < 2$ GeV and $|\eta| < 2$ [44].

Species	β_2	β_3	a_0	R_0
Ru	0.162	0	0.46 fm	5.09 fm
Zr	0.06	0.20	0.52 fm	5.02 fm
difference	$\Delta\beta_2^2$	$\Delta\beta_3^2$	Δa_0	ΔR_0
	0.0226	-0.04	-0.06 fm	0.07 fm

TABLE I. Default values of global nuclear structure parameters in Eq. (1) for ^{96}Ru and ^{96}Zr and the differences between them.

To explore the parametric dependence of the hydrodynamic response, the four parameters of Eq. (1) are varied one at a time relative to a reference point. The β_2 is changed from 0 to 0.1, 0.15 and 0.2; the β_3 is changed from 0 to 0.1, 0.2 and 0.25; the a is varied from 0.52 fm to 0.46 fm, 0.40 fm and 0.34 fm; the R_0 is varied from 5.09 fm to 5.02 fm, 4.8 fm and 4.5 fm. For each case, an independent sample is generated and the v_2 , v_3 and $p(N_{\text{ch}})$ are calculated. The ratios of these observables to those obtained at the reference values are calculated, and the differences from unity, $R_{\mathcal{O}} - 1$, are then scaled according to the actual differences between Ru and Zr listed in Table I. This is done as a function of N_{ch} and the results for all twelve cases (four parameters times three observables) are summarized with various symbols in Fig. 2.

One striking feature is the nearly perfect scaling of $R_{\mathcal{O}}$ over the wide range of parameter values studied, although each case shows its own characteristic N_{ch} -dependent shape. The shapes of these dependences reflect directly the response coefficients c_n in Eq. (3) for each observable. The statistical uncertainties of c_n decrease for larger variation of the WS parameters, implying that the c_n can be determined more precisely by using a larger change of these parameters in the model. This has the benefit of significantly reducing the number of events required in the hydrodynamic model simulation to achieve the desired precision, ideally suitable for the multi-system Bayesian global analyses of heavy-ion collisions [46, 47].

All the WS parameters do not have the same influences on final-state observables. In peripheral and mid-central collisions, the ratio $p(N_{\text{ch}})_{\text{Ru}}/p(N_{\text{ch}})_{\text{Zr}}$ is influenced mostly by the Δa and ΔR_0 , in particular the characteristic broad peak and non-monotonic behavior of the ratio is a clear signature of the influence of Δa [41]. In the most central collisions, the ratio is sensitive to all four parameters, unsurprisingly, due to the exponential decrease of $p(N_{\text{ch}})$ towards larger N_{ch} . The influence of WS parameters on $v_{2,\text{Ru}}/v_{2,\text{Zr}}$ is more complex. 1) in the most central collisions, the ratio is mainly dominated by $\Delta\beta_2^2$ and to a lesser extent by $\Delta\beta_3^2$; 2) in the near-central collisions, the ratio is influenced by a positive contribution from $\Delta\beta_2^2$ and a larger negative contribution from $\Delta\beta_3^2$; 3) in the mid-central and peripheral collisions, the

¹ For higher-order correlators, such as skewness of p_{T} fluctuation and v_n^2 – p_{T} correlation, the leading order term scales with β_n^3 [34].

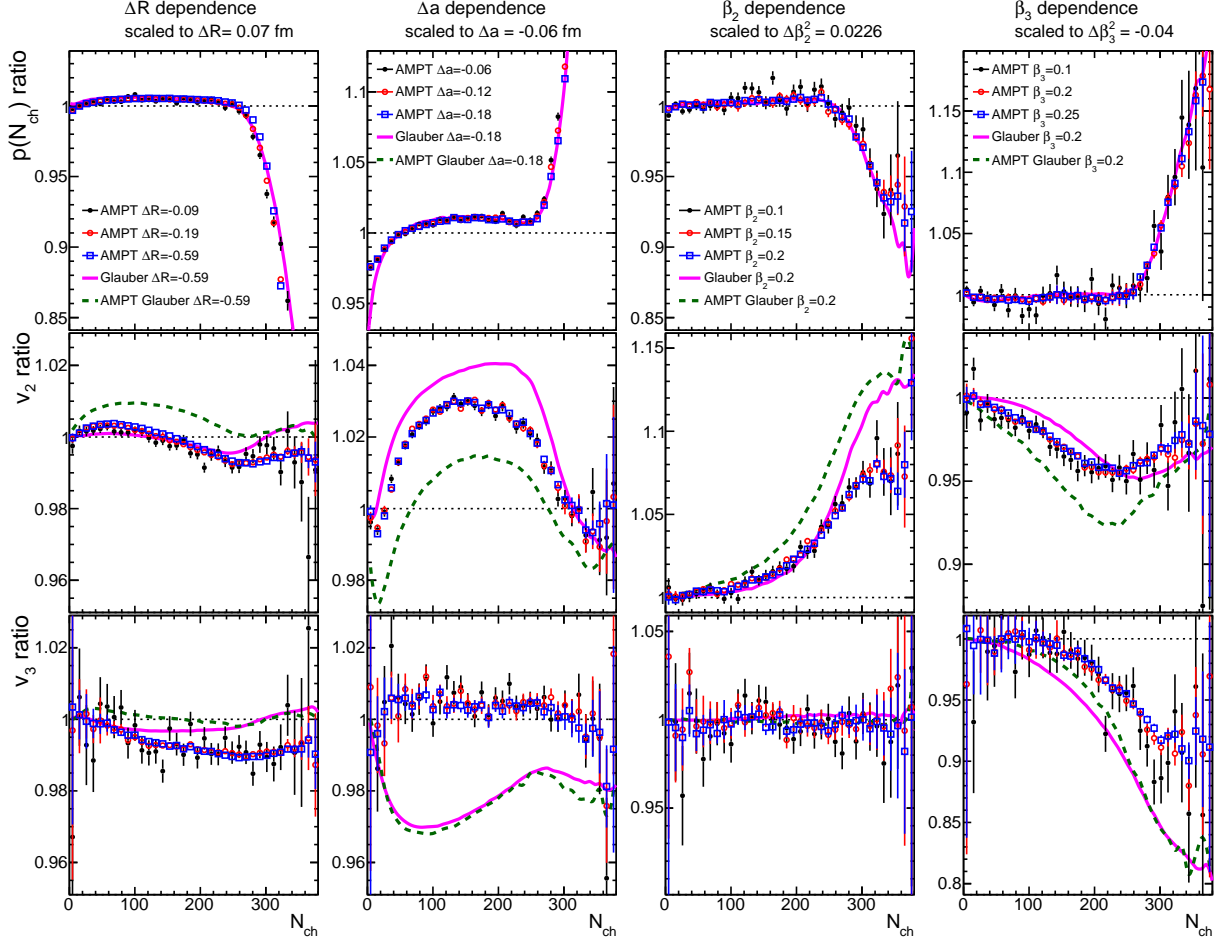


FIG. 2. The four terms of Eq. (3) for parameters R_0 (left column), a (2nd column), β_2 (3rd column) and β_3 (right column) in the AMPT model for ratios of $p(N_{\text{ch}})$ (first row), v_2 (middle row) and v_3 (bottom row). Distribution in each panel is determined for several values of parameters and scaled to the same default value. They are compared with those obtained for quark Glauber model (solid lines) and Glauber model implemented in the AMPT (dashed lines).

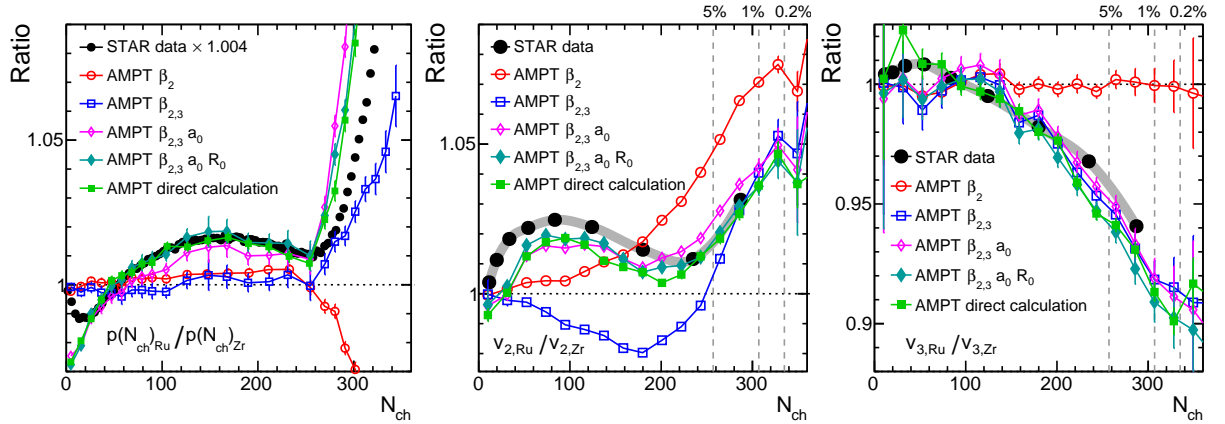


FIG. 3. The ratios of v_2 (left panel), v_3 (middle panel) and $p(N_{\text{ch}})$ (right panel) from AMPT using the default nuclear structure parameters in Table I (labeled “direct calculation”) or calculated step-by-step from the response coefficients shown in Fig. 2 (other symbols). The N_{ch} value from AMPT has been scaled by 1.06 to match the data. Note also that the original STAR v_n ratios [33] were obtained as a function of centrality, but the events with the same average centrality in the two systems have slightly different $\langle N_{\text{ch}} \rangle$. Therefore, a simple interpolation was used to obtain the ratios of v_n at the same N_{ch} [45], which are labelled as “STAR data” in this figure.

impact of Δa is more important; 4) the influence of ΔR_0 is negligible except in the central collisions. Lastly, the ratio $v_{3,\text{Ru}}/v_{3,\text{Zr}}$ is mainly influenced by $\Delta\beta_3^2$, although the ΔR_0 has a modest up to 1% reduction on the ratio over a broad N_{ch} range.

To further understand the behaviors of various response coefficients, we also performed two separate Glauber model calculations. The first calculation is based on the quark Glauber model discussed in Refs. [20, 34], where each nucleon is replaced by three constituent quarks. The distribution of quark-participants $p(N_{\text{quark}})$ generated for the parameter set of ^{96}Ru in Table I is then convoluted with a negative binomial distribution that describes the production of charged particle for each participant, $p_{\text{nbd}}(n) = \frac{(n+m-1)!}{(m-1)!n!} \frac{\bar{n}^n m^m}{(\bar{n}+m)^{n+m}}$, where \bar{n} is the average number of charge particle produced for each participant, and m controls the relative width $\langle (n - \bar{n})^2 \rangle / \bar{n}^2 = 1/\bar{n} + 1/m$. The convoluted distribution is tuned to match the published $p(N_{\text{ch}})_{\text{Ru}}$, giving the best fit values of $\bar{n} = 0.6535$ and $m = 0.7515$. These values are then used to generate the $p(N_{\text{ch}})$ for all other WS parameters. From this, we then calculate the eccentricities ε_n as a function of N_{ch} and obtain the ratios $\varepsilon_{n,\text{Ru}}/\varepsilon_{n,\text{Zr}}$ as an estimator for $v_{n,\text{Ru}}/v_{n,\text{Zr}}$. The second Glauber model calculation is based on the AMPT model itself. This model has a particular way of labeling which nucleon is participating using the HIJING model, from which we can calculate directly $\varepsilon_{n,\text{Ru}}/\varepsilon_{n,\text{Zr}}$ as a function of N_{ch} . We have checked that these ratios from both Glauber models follow the same scaling behavior similar to those shown in Fig. 2. Therefore, only one curve scaled to the default differences is shown for each Glauber model.

The Glauber model results are shown as lines in Fig. 2. The quark Glauber model agrees very well with the ratios of multiplicity distributions from the AMPT model, except in the lowest N_{ch} region for the Δa dependence. The ratios $\varepsilon_{n,\text{Ru}}/\varepsilon_{n,\text{Zr}}$ also show qualitatively, and sometime quantitatively similar N_{ch} dependence trends as the $v_{n,\text{Ru}}/v_{n,\text{Zr}}$, with one exception: $\varepsilon_{3,\text{Ru}}/\varepsilon_{3,\text{Zr}}$ is significantly below unity in the case of $\Delta a = -0.06 \text{ fm}$ [12], with the $v_{3,\text{Ru}}/v_{3,\text{Zr}}$ however slightly above one. This behavior suggests that the development of v_3 is insensitive to the modification of ε_3 by the nucleons at the surface of the nuclei. A comparison between the two Glauber models show similar N_{ch} dependence trends. However, significant differences are observed for $\varepsilon_{2,\text{Ru}}/\varepsilon_{2,\text{Zr}}$, in particular for the responses to ΔR_0 and Δa . These differences are likely related to details of how the participating nucleons are labeled in the AMPT model. Nevertheless, these differences do not affect our main conclusion that the ratios of experimental observables scale nearly perfectly with the differences in the bulk nuclear structure parameters between the isobar systems.

One natural consequence of the scaling relation in Fig. 2 is that it allows us to construct directly the ra-

tios of experimental observables for any values of $\Delta\beta_2^2$, $\Delta\beta_3^2$, Δa and ΔR_0 between the isobar systems, without the need to carry out additional simulations. One could also perform a simultaneous fit of several experimental ratios to obtain the optimal values of WS parameters within a given model framework and expose its limitations. Figure 3 shows a step-by-step construction of the prediction in comparison with the STAR data. From these, one can see clearly the influence of each WS parameter on all three experimental ratios. Each panel also shows the ratio obtained directly from a separate AMPT simulation of $^{96}\text{Ru}+^{96}\text{Ru}$ and $^{96}\text{Zr}+^{96}\text{Zr}$ collisions using the default parameters in the Table I. Excellent agreement is obtained between the construction approach and the direct calculation, attesting to the robustness of our proposed method. This comparison also shows that the AMPT model does not describe the v_2 ratio and $p(N_{\text{ch}})$ ratio at very low N_{ch} region, which might require feature of nucleon distribution beyond what is included in the Wood-Saxon form of Eq. (1) or different models of the initial state [48].

The scaling approach discussed above can be extended to compare collisions of systems with similar but slightly different mass number, ideally along an isotopic chain. As the multiplicity distribution scales approximately with A , the ratios of experimental observable can be obtained as a function of $N_{\text{ch}}/(2A)$ or centrality. The response coefficients c_n in Eq. (3) can then be parameterized in terms of ΔA , which to leading order are expected to scale as $c_n = c_{n;0} + c_{n;1}\Delta A$ (some studies along this line have been done for nuclear deformations [18, 20]). This procedure can be quantified/tested in a given hydrodynamic model and compared to existing $^{197}\text{Au}+^{197}\text{Au}$ and $^{238}\text{U}+^{238}\text{U}$ data. In conjunction with the scaling relations for the nuclear structure parameters discussed above, they will be a powerful tool in understanding the system size dependence of heavy-ion observables.

The scaling approach also provides a clean way to probe the difference between the root mean square radius of neutrons and protons in heavy nuclei, $\Delta r_{np} = R_n - R_p$, known as the neutron skin. Firstly, the mean square radius of nucleon distribution in Eq. (1) can be approximated by $R^2 \approx (\frac{3}{5}R_0^2 + \frac{7}{5}\pi^2 a^2)/(1 + \frac{5}{4\pi^2} \sum_n \beta_n^2)$ [49]. From this, the neutron skin can be expressed as the differences between nucleon distribution and proton distribution:

$$\Delta r_{np} \approx D(1 + \frac{D\delta}{2R}),$$

$$D = \frac{R^2 - R_p^2}{R(\delta+1)} \approx \frac{3(R_0^2 - R_{0,p}^2) + 7\pi^2(a^2 - a_p^2)}{\sqrt{15}R_0\sqrt{1 + \frac{7\pi^2}{3}\frac{a^2}{R_0^2}(1 + \delta + \frac{5}{8\pi^2}\sum_n \beta_n^2)}} \quad (4)$$

where $\delta = (N - Z)/A$ is the asymmetry parameter and $R_{0,p}$ and a_p are the well-measured WS parameters for the proton distribution [42]. Simple algebraic manipulation shows that the ΔR_0 and Δa obtained from isobar collisions can be related to the differences in their neutron

skins,

$$\Delta(\Delta r_{np}) \approx -\overline{\Delta r_{np}} \left(\frac{\Delta\delta}{1+\delta} + \frac{\Delta R_0}{R_0} \right) + \frac{\Delta Y - \frac{7\pi^2}{3} \frac{\bar{a}^2}{R_0^2} \left(\frac{\Delta Y}{2} + \bar{Y} \left(\frac{\Delta a}{\bar{a}} - \frac{\Delta R_0}{R_0} \right) \right)}{\sqrt{15} R_0 (1 + \delta + \frac{5}{8\pi^2} \sum_n \bar{\beta}_n^2)}, \quad (5)$$

where \bar{x} represents the average of quantity x between the two systems, and $Y \equiv 3(R_0^2 - R_{0,p}^2) + 7\pi^2(a^2 - a_p^2)$. The term associated with $\overline{\Delta r_{np}}$ can be dropped if we ignore change of δ and R_0 , which is typically a few percent to ten percent level of $\overline{\Delta r_{np}}$ for isobar systems. The numerator of Eq. 5 is dominated by $\Delta Y = 6(\bar{R}_0 \Delta R_0 - \bar{R}_{0p} \Delta R_{0p}) + 14\pi^2(\bar{a} \Delta a - \bar{a}_p \Delta a_p)$, but the remaining term is on the order of $\frac{7\pi^2}{3} \frac{\bar{a}^2}{R_0^2} \sim 23(0.5/5)^2 = 23\%$ of ΔY , also significant.

We checked that the Eq. (5) is accurate within 2% using the set of parameters for ^{96}Ru and ^{96}Zr listed in Ref. [41].

Eq. (5) is derived assuming small differences in WS parameters, which is valid for any pairs of systems with similar mass number. It shows that the difference in neutron skin is sensitive to both ΔR_0 (skin-type contribution) and Δa (halo-type contribution) [43]. In addition to isobar systems, another useful application of Eq. (5) and Eq. (3) (after correcting for the A dependence) is along isotopic chains around major shells, such as the Sn and Pb isotopes, for which an increase of neutron skin is expected [6]. Since observables in heavy-ion collisions can constrain the values of ΔR_0 and Δa , together with the well-measured $\Delta R_{0,p}$ and Δa_p for the proton distribution, we could separate the skin-type or halo-type contributions via Eq. (5). This could constrain the symmetry energy contribution to the equation of state (EOS) at near 2/3 of the normal nuclear density [50] which is a quantity of fundamental importance in nuclear- and astro-physics [51, 52]: an increased contribution to the neutron skin associated with ΔR_0 (a_0) would imply a stiffer (softer) EOS [53].

Our discussion ignores isospin-dependent dynamical effects in the initial- and final-state of the collisions. This is a good approximation at top RHIC energy, since the matter produced is essentially net-baryon free and isospin symmetric, as reflected by the fact that the v_n and mean p_T of identified particles and their antiparticles are similar [54, 55]. Such isospin-dependent effects are more important at lower energies ($\sqrt{s_{NN}} < 10$ GeV) [52, 56, 57]. It will be of great interest to study the $\sqrt{s_{NN}}$ dependence of the scaling behavior in the ratio of heavy-ion observables.

In summary, we have presented a new approach to constrain the collective nuclear structure parameters in high-energy heavy-ion isobar collisions. We have found that the changes in the final-state observables v_2 , v_3 and $p(N_{ch})$ follow a simple dependences on the variation of these parameters. The coefficients of these variations can be determined precisely in a given model of heavy-ion col-

lisions, which can be used to make predictions of observables at other parameter values. This scaling behavior is particular useful in analyzing the ratios between isobar systems, such as $^{96}\text{Ru} + ^{96}\text{Ru}$ and $^{96}\text{Zr} + ^{96}\text{Zr}$ collisions measured by the STAR experiment [33]. We have shown that the STAR data can precisely constrain the differences of quadrupole deformation $\Delta\beta_2^2 = \beta_{2,\text{Ru}}^2 - \beta_{2,\text{Zr}}^2$, octupole deformation $\Delta\beta_3^2 = \beta_{3,\text{Ru}}^2 - \beta_{3,\text{Zr}}^2$, nuclear radius $\Delta R_0 = R_{0,\text{Ru}} - R_{0,\text{Zr}}$ and surface diffuseness $\Delta a = a_{\text{Ru}} - a_{\text{Zr}}$, therefore making isobar collisions a precise tool for accessing bulk nuclear structure parameters. In particular, the extracted values of ΔR_0 and Δa , together with well-measured charge distribution, can constrain the difference in the neutron skin between large isobar systems. These results demonstrate the unique opportunities offered by relativistic collisions of isobars as a tool to perform inter-disciplinary nuclear physics studies, which we hope will be pursued in future by collisions of several isobar pairs in collider facilities.

Acknowledgements: We thank Giuliano Giacalone, Che-Ming Ko, Bao-An Li and Jun Xu for careful reading and valuable comments on the manuscript. This work is supported by DOE DEFG0287ER40331.

* Correspond to jiangyong.jia@stonybrook.edu

† Correspond to chun-jian.zhang@stonybrook.edu

- [1] Takashi Nakatsukasa, Kenichi Matsuyanagi, Masayuki Matsuo, and Kazuhiro Yabana, “Time-dependent density-functional description of nuclear dynamics,” *Rev. Mod. Phys.* **88**, 045004 (2016), [arXiv:1606.04717 \[nucl-th\]](https://arxiv.org/abs/1606.04717).
- [2] Witold Nazarewicz, “Challenges in Nuclear Structure Theory,” *J. Phys. G* **43**, 044002 (2016), [arXiv:1603.02490 \[nucl-th\]](https://arxiv.org/abs/1603.02490).
- [3] P. Möller, A. J. Sierk, T. Ichikawa, and H. Sagawa, “Nuclear ground-state masses and deformations: FRDM(2012),” *Atom. Data Nucl. Data Tabl.* **109-110**, 1–204 (2016), [arXiv:1508.06294 \[nucl-th\]](https://arxiv.org/abs/1508.06294).
- [4] Yuchen Cao, Sylvester E. Agbemava, Anatoli V. Afanasjev, Witold Nazarewicz, and Erik Olsen, “Landscape of pear-shaped even-even nuclei,” *Phys. Rev. C* **102**, 024311 (2020), [arXiv:2004.01319 \[nucl-th\]](https://arxiv.org/abs/2004.01319).
- [5] I. Angeli and K. P. Marinova, “Table of experimental nuclear ground state charge radii: An update,” *Atom. Data Nucl. Data Tabl.* **99**, 69–95 (2013).
- [6] M. Centelles, X. Roca-Maza, X. Vinas, and M. Warda, “Nuclear symmetry energy probed by neutron skin thickness of nuclei,” *Phys. Rev. Lett.* **102**, 122502 (2009), [arXiv:0806.2886 \[nucl-th\]](https://arxiv.org/abs/0806.2886).
- [7] I. Tanihata, H. Hamagaki, O. Hashimoto, Y. Shida, N. Yoshikawa, K. Sugimoto, O. Yamakawa, T. Kobayashi, and N. Takahashi, “Measurements of Interaction Cross-Sections and Nuclear Radii in the Light p Shell Region,” *Phys. Rev. Lett.* **55**, 2676–2679 (1985).
- [8] A. Rosenhauer, H. Stocker, J. A. Maruhn, and W. Greiner, “Influence of shape fluctuations in rela-

- tivistic heavy ion collisions,” *Phys. Rev. C* **34**, 185–190 (1986).
- [9] Bao-An Li, “Uranium on uranium collisions at relativistic energies,” *Phys. Rev. C* **61**, 021903 (2000), [arXiv:nucl-th/9910030](#).
- [10] Ulrich W. Heinz and Anthony Kuhlman, “Anisotropic flow and jet quenching in ultrarelativistic U + U collisions,” *Phys. Rev. Lett.* **94**, 132301 (2005), [arXiv:nucl-th/0411054](#).
- [11] Peter Filip, Richard Lednicky, Hiroshi Masui, and Nu Xu, “Initial eccentricity in deformed $^{197}\text{Au} + ^{197}\text{Au}$ and $^{238}\text{U} + ^{238}\text{U}$ collisions at $\sqrt{s_{\text{NN}}} = 200$ GeV at the BNL Relativistic Heavy Ion Collider,” *Phys. Rev. C* **80**, 054903 (2009).
- [12] Q. Y. Shou, Y. G. Ma, P. Sorensen, A. H. Tang, F. Videbæk, and H. Wang, “Parameterization of Deformed Nuclei for Glauber Modeling in Relativistic Heavy Ion Collisions,” *Phys. Lett. B* **749**, 215–220 (2015), [arXiv:1409.8375 \[nucl-th\]](#).
- [13] Andy Goldschmidt, Zhi Qiu, Chun Shen, and Ulrich Heinz, “Collision geometry and flow in uranium + uranium collisions,” *Phys. Rev. C* **92**, 044903 (2015), [arXiv:1507.03910 \[nucl-th\]](#).
- [14] Giuliano Giacalone, Jacquelyn Noronha-Hostler, Matthew Luzum, and Jean-Yves Ollitrault, “Hydrodynamic predictions for 5.44 TeV Xe+Xe collisions,” *Phys. Rev. C* **97**, 034904 (2018), [arXiv:1711.08499 \[nucl-th\]](#).
- [15] Giuliano Giacalone, “Observing the deformation of nuclei with relativistic nuclear collisions,” *Phys. Rev. Lett.* **124**, 202301 (2020), [arXiv:1910.04673 \[nucl-th\]](#).
- [16] Giuliano Giacalone, “Constraining the quadrupole deformation of atomic nuclei with relativistic nuclear collisions,” *Phys. Rev. C* **102**, 024901 (2020), [arXiv:2004.14463 \[nucl-th\]](#).
- [17] Giuliano Giacalone, Jiangyong Jia, and Vittorio Somà, “Accessing the shape of atomic nuclei with relativistic collisions of isobars,” *Phys. Rev. C* **104**, L041903 (2021), [arXiv:2102.08158 \[nucl-th\]](#).
- [18] Giuliano Giacalone, Jiangyong Jia, and Chunjian Zhang, “The impact of nuclear deformation on relativistic heavy-ion collisions: assessing consistency in nuclear physics across energy scales,” (2021), [arXiv:2105.01638 \[nucl-th\]](#).
- [19] Jiangyong Jia, Shengli Huang, and Chunjian Zhang, “Constraining nuclear quadrupole deformation from correlation of elliptic flow and transverse momentum in nuclear collisions,” (2021), [arXiv:2105.05713 \[nucl-th\]](#).
- [20] Jiangyong Jia, “Shape of atomic nuclei in heavy ion collisions,” (2021), [arXiv:2106.08768 \[nucl-th\]](#).
- [21] Benjamin Bally, Michael Bender, Giuliano Giacalone, and Vittorio Somà, “Evidence of the triaxial structure of ^{129}Xe at the Large Hadron Collider,” (2021), [arXiv:2108.09578 \[nucl-th\]](#).
- [22] L. Adamczyk *et al.* (STAR), “Azimuthal anisotropy in U+U and Au+Au collisions at RHIC,” *Phys. Rev. Lett.* **115**, 222301 (2015), [arXiv:1505.07812 \[nucl-ex\]](#).
- [23] S. Acharya *et al.* (ALICE), “Anisotropic flow in Xe-Xe collisions at $\sqrt{s_{\text{NN}}} = 5.44$ TeV,” *Phys. Lett. B* **784**, 82–95 (2018), [arXiv:1805.01832 \[nucl-ex\]](#).
- [24] Albert M Sirunyan *et al.* (CMS), “Charged-particle angular correlations in XeXe collisions at $\sqrt{s_{\text{NN}}} = 5.44$ TeV,” *Phys. Rev. C* **100**, 044902 (2019), [arXiv:1901.07997 \[hep-ex\]](#).
- [25] Georges Aad *et al.* (ATLAS), “Measurement of the azimuthal anisotropy of charged-particle production in Xe+Xe collisions at $\sqrt{s_{\text{NN}}} = 5.44$ TeV with the ATLAS detector,” *Phys. Rev. C* **101**, 024906 (2020), [arXiv:1911.04812 \[nucl-ex\]](#).
- [26] Jiangyong Jia, “Nuclear deformation effects via Au+Au and U+U collisions from STAR,” Contribution to the VIth International Conference on the Initial Stages of High-Energy Nuclear Collisions, January 2021, <https://indico.cern.ch/event/854124/contributions/4135480/>.
- [27] Wit Busza, Krishna Rajagopal, and Wilke van der Schee, “Heavy Ion Collisions: The Big Picture, and the Big Questions,” *Ann. Rev. Nucl. Part. Sci.* **68**, 339–376 (2018), [arXiv:1802.04801 \[hep-ph\]](#).
- [28] Wataru Horiuchi, “Single-particle decomposition of nuclear surface diffuseness,” (2021), [arXiv:2110.04982 \[nucl-th\]](#).
- [29] Patrick Carzon, Skandaprasad Rao, Matthew Luzum, Matthew Sievert, and Jacquelyn Noronha-Hostler, “Possible octupole deformation of ^{208}Pb and the ultracentral v_2 to v_3 puzzle,” (2020), [arXiv:2007.00780 \[nucl-th\]](#).
- [30] Derek Teaney and Li Yan, “Non linearities in the harmonic spectrum of heavy ion collisions with ideal and viscous hydrodynamics,” *Phys. Rev. C* **86**, 044908 (2012), [arXiv:1206.1905 \[nucl-th\]](#).
- [31] H. Niemi, K. J. Eskola, and R. Paatelainen, “Event-by-event fluctuations in a perturbative QCD + saturation + hydrodynamics model: Determining QCD matter shear viscosity in ultrarelativistic heavy-ion collisions,” *Phys. Rev. C* **93**, 024907 (2016), [arXiv:1505.02677 \[hep-ph\]](#).
- [32] Hanlin Li, Hao-jie Xu, Jie Zhao, Zi-Wei Lin, Hanzhong Zhang, Xiaobao Wang, Caiwan Shen, and Fuqiang Wang, “Multiphase transport model predictions of isobaric collisions with nuclear structure from density functional theory,” *Phys. Rev. C* **98**, 054907 (2018), [arXiv:1808.06711 \[nucl-th\]](#).
- [33] Mohamed Abdallah *et al.* (STAR), “Search for the Chiral Magnetic Effect with Isobar Collisions at $\sqrt{s_{\text{NN}}} = 200$ GeV by the STAR Collaboration at RHIC,” (2021), [arXiv:2109.00131 \[nucl-ex\]](#).
- [34] Jiangyong Jia, “Probing triaxial deformation of atomic nuclei in high-energy heavy ion collisions,” (2021), [arXiv:2109.00604 \[nucl-th\]](#).
- [35] Zi-Wei Lin, Che Ming Ko, Bao-An Li, Bin Zhang, and Subrata Pal, “A Multi-phase transport model for relativistic heavy ion collisions,” *Phys. Rev. C* **72**, 064901 (2005), [arXiv:nucl-th/0411110 \[nucl-th\]](#).
- [36] Jun Xu and Che Ming Ko, “Pb-Pb collisions at $\sqrt{s_{\text{NN}}} = 2.76$ TeV in a multiphase transport model,” *Phys. Rev. C* **83**, 034904 (2011), [arXiv:1101.2231 \[nucl-th\]](#).
- [37] Mohamed Abdallah *et al.* (STAR), “Azimuthal anisotropy measurements of strange and multistrange hadrons in U + U collisions at $\sqrt{s_{\text{NN}}} = 193$ GeV at the BNL Relativistic Heavy Ion Collider,” *Phys. Rev. C* **103**, 064907 (2021), [arXiv:2103.09451 \[nucl-ex\]](#).
- [38] Chunjian Zhang and Jiangyong Jia, “Evidence of quadrupole and octupole deformations in $^{96}\text{Zr} + ^{96}\text{Zr}$ and $^{96}\text{Ru} + ^{96}\text{Ru}$ collisions at ultra-relativistic energies,” (2021), [arXiv:2109.01631 \[nucl-th\]](#).
- [39] Guo-Liang Ma and Adam Bzdak, “Long-range azimuthal correlations in proton–proton and proton–nucleus collisions from the incoherent scattering of partons,” *Phys. Lett. B* **739**, 209–213 (2014), [arXiv:1404.4129 \[hep-ph\]](#).
- [40] Adam Bzdak and Guo-Liang Ma, “Elliptic and triangu-

- lar flow in p +Pb and peripheral Pb+Pb collisions from parton scatterings,” *Phys. Rev. Lett.* **113**, 252301 (2014), [arXiv:1406.2804 \[hep-ph\]](#).
- [41] Hao-jie Xu, Hanlin Li, Xiaobao Wang, Caiwan Shen, and Fuqiang Wang, “Determine the neutron skin type by relativistic isobaric collisions,” *Phys. Lett. B* **819**, 136453 (2021), [arXiv:2103.05595 \[nucl-th\]](#).
- [42] G. Fricke, C. Bernhard, K. Heilig, L. A. Schaller, L. Schellenberg, E. B. Shera, and C. W. de Jager, “Nuclear Ground State Charge Radii from Electromagnetic Interactions,” *Atomic Data and Nuclear Data Tables* **60**, 177 (1995).
- [43] A. Trzcinska, J. Jastrzebski, P. Lubinski, F. J. Hartmann, R. Schmidt, T. von Egidy, and B. Klos, “Neutron density distributions deduced from anti-protonic atoms,” *Phys. Rev. Lett.* **87**, 082501 (2001).
- [44] Georges Aad *et al.* (ATLAS), “Measurement of the azimuthal anisotropy for charged particle production in $\sqrt{s_{NN}} = 2.76$ TeV lead-lead collisions with the ATLAS detector,” *Phys. Rev. C* **86**, 014907 (2012), [arXiv:1203.3087 \[hep-ex\]](#).
- [45] Wang Gang, Contribution to The 6th International Conference on Chirality, Vorticity and Magnetic Field in Heavy Ion Collisions, November 2021, <https://indico.bnl.gov/event/7012/contributions/56441>.
- [46] Govert Nijs, Wilke van der Schee, Umut Gürsoy, and Raimond Snellings, “Transverse Momentum Differential Global Analysis of Heavy-Ion Collisions,” *Phys. Rev. Lett.* **126**, 202301 (2021), [arXiv:2010.15130 \[nucl-th\]](#).
- [47] D. Everett *et al.* (JETSCAPE), “Phenomenological constraints on the transport properties of QCD matter with data-driven model averaging,” *Phys. Rev. Lett.* **126**, 242301 (2021), [arXiv:2010.03928 \[hep-ph\]](#).
- [48] Giuliano Giacalone, Björn Schenke, and Chun Shen, “Constraining the nucleon size with relativistic nuclear collisions,” (2021), [arXiv:2111.02908 \[nucl-th\]](#).
- [49] Aage Bohr and Ben R Mottelson, eds., *Nuclear Structure* (World Scientific, 1998).
- [50] Jun Xu, Wen-Jie Xie, and Bao-An Li, “Bayesian inference of nuclear symmetry energy from measured and imagined neutron skin thickness in $^{116,118,120,122,124,130,132}\text{Sn}$, ^{208}Pb , and ^{48}Ca ,” *Phys. Rev. C* **102**, 044316 (2020), [arXiv:2007.07669 \[nucl-th\]](#).
- [51] James M. Lattimer and Maddapa Prakash, “Neutron Star Observations: Prognosis for Equation of State Constraints,” *Phys. Rept.* **442**, 109–165 (2007), [arXiv:astro-ph/0612440](#).
- [52] Bao-An Li, Lie-Wen Chen, and Che Ming Ko, “Recent Progress and New Challenges in Isospin Physics with Heavy-Ion Reactions,” *Phys. Rept.* **464**, 113–281 (2008), [arXiv:0804.3580 \[nucl-th\]](#).
- [53] M. Centelles, X. Roca-Maza, X. Vinas, and M. Warda, “Origin of the neutron skin thickness of ^{208}Pb in nuclear mean-field models,” *Phys. Rev. C* **82**, 054314 (2010), [arXiv:1010.5396 \[nucl-th\]](#).
- [54] L. Adamczyk *et al.* (STAR), “Observation of an Energy-Dependent Difference in Elliptic Flow between Particles and Antiparticles in Relativistic Heavy Ion Collisions,” *Phys. Rev. Lett.* **110**, 142301 (2013), [arXiv:1301.2347 \[nucl-ex\]](#).
- [55] L. Adamczyk *et al.* (STAR), “Bulk Properties of the Medium Produced in Relativistic Heavy-Ion Collisions from the Beam Energy Scan Program,” *Phys. Rev. C* **96**, 044904 (2017), [arXiv:1701.07065 \[nucl-ex\]](#).
- [56] F. Rami *et al.* (FOPI), “Isospin tracing: A Probe of nonequilibrium in central heavy ion collisions,” *Phys. Rev. Lett.* **84**, 1120–1123 (2000), [arXiv:nucl-ex/9908014](#).
- [57] X. Lopez *et al.* (FOPI), “Isospin dependence of relative yields of K^+ and K^0 mesons at 1.528-AGeV,” *Phys. Rev. C* **75**, 011901 (2007), [arXiv:nucl-ex/0701006](#).

SUPPLEMENTAL MATERIALS

To show how Eq. (5) is derived, we note that the ms radii for nucleon, neutron and proton distributions are related by

$$R^2 = \frac{1+\delta}{2} R_n^2 + \frac{1-\delta}{2} R_p^2. \quad (6)$$

This leads to $\Delta r_{np} \frac{R_n+R_p}{2} = \frac{R^2-R_p^2}{1+\delta}$, and together with the approximation $R_n + R_p \approx 2R - \delta \Delta r_{np}$, we get

$$\Delta r_{np} \left(1 - \frac{\Delta r_{np} \delta}{2R}\right) = \frac{R^2 - R_p^2}{R(1+\delta)} \equiv D. \quad (7)$$

From this we obtain Eq. (4). To derive Eq. (5), we plug the expression for D in Eq. (4) and obtain the following approximate expression,

$$\Delta r_{np} \sqrt{15} R_0 \left(1 + \delta + \frac{5}{8\pi^2} \sum_n \beta_n^2\right) \approx (3(R_0^2 - R_{0,p}^2) + 7\pi^2(a^2 - a_p^2)) \left(1 - \frac{7\pi^2}{6} \frac{a^2}{R_0^2}\right), \quad (8)$$

where we have ignored the high-order terms $\frac{\Delta r_{np} \delta}{2R}$ on the left hand side (lhs) and $\mathcal{O}(\frac{a^4}{R_0^4})$ on the right hand side (rhs), which are much less than 1% for medium and large nuclei. We now consider the difference of two such expressions for two isobars, labelled by “1” and “2”, respectively. We shall use the relations $x_1 y_1 - x_2 y_2 = \Delta x \bar{y} + \Delta y \bar{x}$ and $x_1 y_1 z_1 - x_2 y_2 z_2 = \Delta x \bar{y} \bar{z} + \Delta y \bar{x} \bar{z} + \Delta z \bar{x} \bar{y} + \frac{1}{4} \Delta x \Delta y \Delta z$, where $\Delta x = x_1 - x_2$ and $\bar{x} = (x_1 + x_2)/2$ etc. Then, the lhs of Eq. (8) can be written as,

$$\begin{aligned} \Delta(\text{lhs})/\sqrt{15} &= \Delta \left[\Delta r_{np} R_0 \left(1 + \delta + \frac{5}{8\pi^2} \sum_n \beta_n^2\right) \right] \\ &\approx \Delta(\Delta r_{np}) \bar{R}_0 (1 + \bar{\delta} + \frac{5}{8\pi^2} \sum_n \bar{\beta}_n^2) \\ &\quad + \bar{\Delta r}_{np} \bar{R}_0 \left(\frac{\Delta R_0}{\bar{R}_0} (1 + \bar{\delta}) + \Delta\delta + \frac{5}{8\pi^2} \sum_n \Delta\beta_n^2 \right). \end{aligned} \quad (9)$$

For the rhs of Eq. (8), it can be written as,

$$\begin{aligned} \Delta(\text{rhs}) &= \Delta \left[(3(R_0^2 - R_{0,p}^2) + 7\pi^2(a^2 - a_p^2)) \left(1 - \frac{7\pi^2}{6} \frac{a^2}{R_0^2}\right) \right] \\ &= \Delta Y - \frac{7\pi^2}{3} \frac{\bar{a}^2}{\bar{R}_0^2} \left(\frac{\Delta Y}{2} + \bar{Y} \left(\frac{\Delta a}{\bar{a}} - \frac{\Delta R_0}{\bar{R}_0} \right) \right), \end{aligned} \quad (10)$$

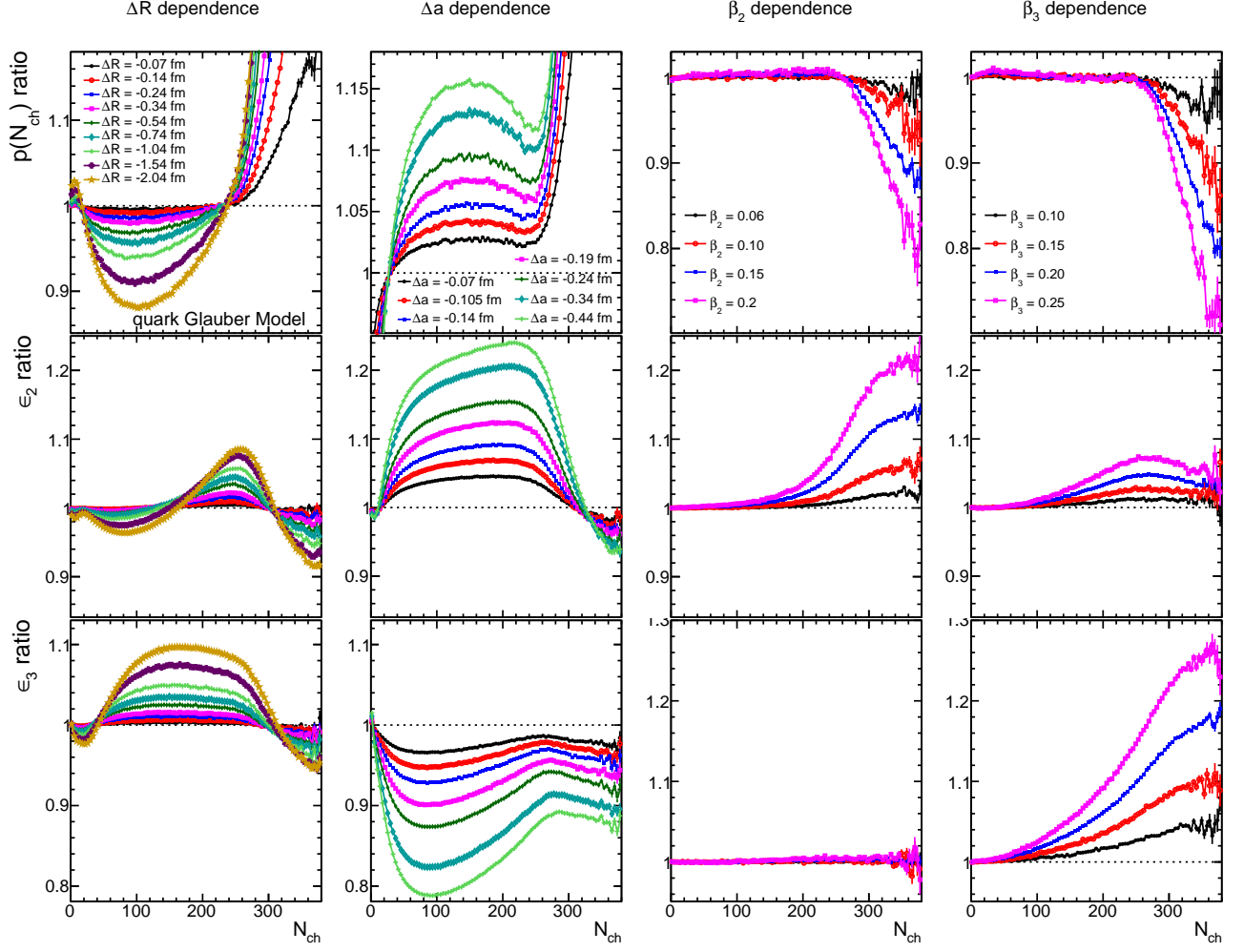


FIG. 4. The four response coefficients of Eq. (3) for variation of nuclear structure parameters R_0 (left column), a (2nd column), β_2 (third column) and β_3 (right column) in the quark Glauber model for ratios of $p(N_{\text{ch}})$ (first row), ε_2 (middle row) and ε_3 (bottom row). Each coefficient in each panel is determined for several values of the parameters and scaled to the same default value.

with $Y \equiv 3(R_0^2 - R_{0,p}^2) + 7\pi^2(a^2 - a_p^2)$. Eq. (5) is then obtained by combining Eq. (9) and Eq. (10).

Figure 4 shows the ratios of $p(N_{\text{ch}})$, ε_2 and ε_3 obtained in the quark Glauber model for several values of R_0 , a , β_2 and β_3 relative to the default. The corresponding ratios

after being scaled to the default variation as listed in Table I are shown in Fig. 5. Some small deviation from this scaling is observed only when the variations are very large.

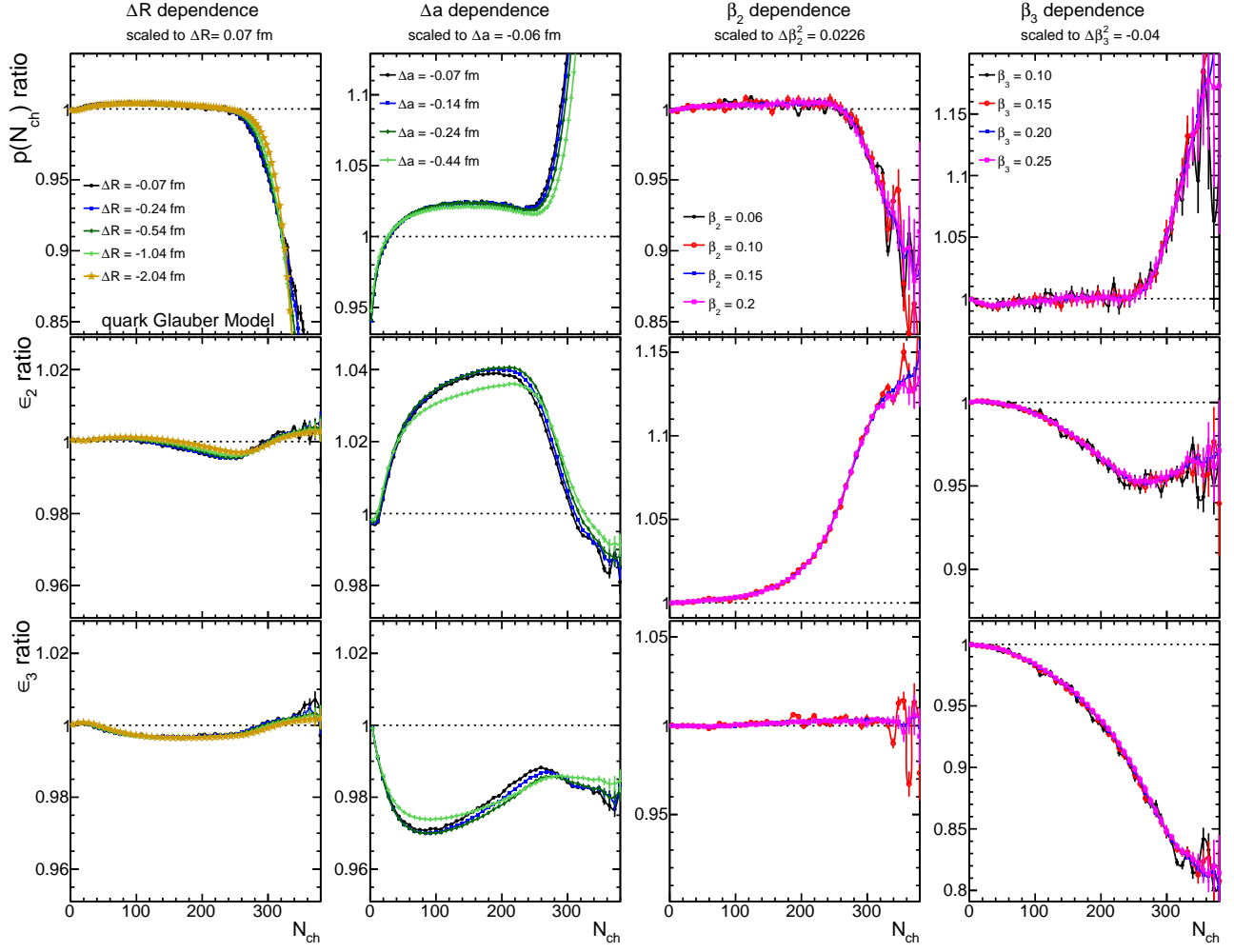


FIG. 5. Information in Fig. 4 scaled to the default variation in the nuclear structure parameters as indicated in the top of each column. Only selected cases are shown for variations in parameters R_0 and a in order to make the plots less busy.